EUROFUSION WPS1-PR(16) 15581

T. Sunn Pedersen et al.

# A stellar(ator) comeback?

Preprint of Paper to be submitted for publication in Nature

This work has been carried out within the framework of the EUROfusion Consortium and has received funding from the Euratom research and training programme 2014-2018 under grant agreement No 633053. The views and opinions expressed herein do not necessarily reflect those of the European Commission.

# A stellar(ator) comeback?

T. Sunn Pedersen[a,b], M. Otte[a], S. Lazerson[c], P. Helander[a,b], S. Bozhenkov[a], C. Biedermann[a], T. Klinger[a,b], R. Wolf[a,c], H.-S. Bosch[a,b] and the Wendelstein 7-X Team

[a] *Max Planck Institute for Plasma Physics, Greifswald, Germany*

[b] *Ernst-Moritz-Arndt University, Greifswald, Germany*

[c] *Princeton Plasma Physics Laboratory, Princeton, NJ, USA*

[d] *Technical University Berlin, Germany*

February 22, 2016

**Abstract**

Fusion energy research has in the past 40 years focussed primarily on the tokamak concept, but recent advances in plasma theory and computational power have led to renewed interest in stellarators. The largest and most sophisticated stellarator in the world, Wendelstein 7-X (W7-X), has just started operation, with the aim to show that the earlier weaknesses of this concept have been addressed successfully, and that the intrinsic advantages of the concept persist, also at plasma parameters approaching those of a future fusion power plant. Its first physics results were obtained before plasma operation: the experimental confirmation of the carefully tailored topology of nested magnetic surfaces needed for good confinement of high-temperature plasma, and experimental confirmation that deviations are smaller than one part in 100,000.

## 1 Magnetic confinement fusion and stellarators

Fusion has the potential to cover the energy needs of the world's population into the distant future. Lawson showed in 1957 that magnetic confinement fusion based on deuterium-tritium fusion can work as a net energy source if one achieves a sufficiently high triple product, $n_i T_i \tau_E > 4 * 10^{21}$ keV m$^{-3}$ s for the plasma, approximately valid for ion temperatures $T_i$ in the range 10-40 keV [1].

Here $n_i$ is the ion density, and $\tau_E$ is the energy confinement time, which for a typical operating point in magnetic fusion reactor studies is a few seconds. In one second, a deuterium ion moves on the order of 1000 km due to its thermal speed in that temperature range. Confinement due to size alone is thus not feasible. The most successful approach to date is to use a magnetic field for confinement: Since the charged particles of the plasma gyrate around and free-stream along magnetic field lines, and the radius of the gyration around the field is very small when the field is a few Tesla, a charged particle can be thought of as being approximately tied to the field line around which it gyrates, and one need only keep track of the centre of its gyration, the guiding centre, and not the gyration itself. The guiding centres move only comparatively slowly across the magnetic field. Thus, a magnetic field thus confines plasma in the directions across the field lines quite well, but confinement along the field can at best be partial. To avoid fast losses along the field, the field lines can be bent around to stay within a closed volume, so that they do not intersect material objects. This way, the total size of the magnetic "cage" for a fusion plasma can be held to something of order 20 meters.

A successful magnetic confinement concept, to date second only to the tokamak, is the stellarator. In a stellarator, nested toroidal magnetic surfaces are created from external magnetic coils,

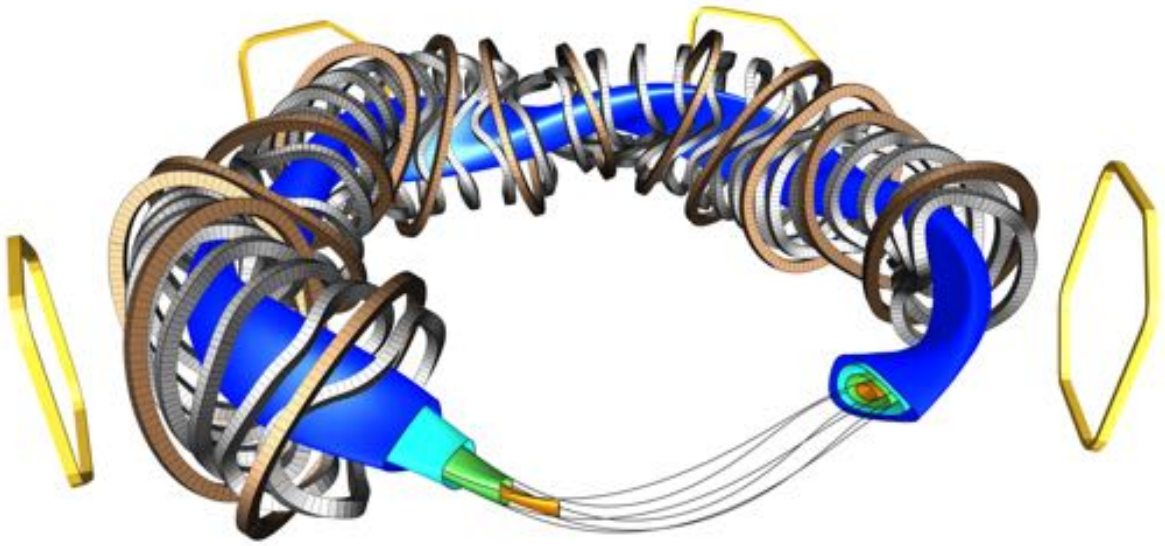

**Figure 1:** The nested magnetic surfaces are shown in different colours in this CAD rendering, together with a representative magnetic field line that lies on the green surface. The coil sets that create the magnetic surfaces are also shown. Some parts are left out of the rendering, allowing for a view of the nested surfaces (left) and a Poincaré section of the shown surfaces (right). Four out of the five external trim coils are shown in yellow.

see Figure 1. Each magnetic field line meanders around on its magnetic surface; it never leaves it. In general, if one follows a field line from one point on a magnetic surface, one never comes back to the same *exact* location. Instead, one covers the surface, coming infinitely close to any point of the surface. As a consequence of the fast motion along the magnetic field, and the slow motion perpendicular to it, the plasma takes the shape of the magnetic surfaces – the plasma density and temperatures are close to uniform on each surface, whereas strong gradients can be sustained from the inner to the outer magnetic surfaces: In large magnetic fusion experiments, temperatures exceeding 100 million degrees K can be sustained on the inner surfaces, simultaneously with having plasma on the outermost surfaces with temperatures below 1 million K, less than a metre away from the hot core. Plasmas for magnetic fusion are tenuous – of order a million times thinner than the air pressure. The heat losses for the plasma and the associated heat loads for the plasma-facing components (PFCs) can be acceptable at 1 MK and some MW/m$^2$, if care is taken in the design of the magnetic topology and the PFCs.

The concept of nested, toroidal magnetic surfaces is not only used in tokamaks and stellarators. Several other magnetic-surface concepts are being, or have been, pursued, e.g. the reversed-field pinch (RFP) [2]. The stellarator is different in that both the toroidal and the poloidal field components - which together create the magnetic surface topology - are created from currents in external coils. In the tokamak and the RFP, a strong toroidal current driven within the plasma is needed to generate the poloidal magnetic-field component. The stellarator's lack of a strong current parallel

to the magnetic field greatly reduces macroscopic plasma instabilities, and it eliminates the need for steady-state current drive. This makes it a more stable configuration, capable of steady-state operation. These are important advantages for a power plant.
The stellarator concept is about as old as magnetic confinement fusion research itself. It was invented by Lyman Spitzer in 1951 and was first developed in secret under the code-name Project Matterhorn. The concept was published 7 years later, after Project Matterhorn was declassified [3]. So why did it fall behind? And why do some believe that it is about to have a comeback?

Plasma confinement in early stellarators was disappointing. This was due to poorly confined particle orbits - many of the guiding-centre trajectories were not fully confined, even though the magnetic field lines were. If each guiding centre were to stay exactly on the magnetic field line it starts out on, the magnetic surfaces would guarantee good confinement. But for all toroidal magnetic systems, the orbits deviate from the field lines, since the guiding centres *drift* perpendicular to the magnetic field. This is due to the field-line curvature and magnetic field strength inhomogeneities inherent to the toroidal magnetic topology. The drift is both tiny and large: A typical number is 100 m/s, 10,000 times slower than the parallel motion, but it can take the particle from the core to the plasma wall in much less than 1/10 of a second, if the drifts do not average out or stay within the magnetic surface but instead carry the particle from the inner to the outer magnetic surfaces. This was the case in early stellarator experiments. The tokamak and the RFP do not suffer from this problem since their toroidal symmetry makes the guiding centre drifts average out for all particles and therefore only cause minor excursions from the magnetic surface.
Advances in plasma theory, in particular in the 1980's and 1990's, allowed the development of stellarator magnetic field configurations that display greatly improved confinement (see eg. [4, 5]), reducing the prompt single-particle losses to a level sufficiently small that it is predicted to be compatible with an economically feasible fusion power plant. The optimisation itself, as well as the associated design of coils that realise the optimised magnetic fields, requires computer power that only became available in the 80's. The first generation of optimised stellarators started operation in the 1990's, and confirmed many of the expected improvements [6, 7]. These devices were, however, too small to reach the high ion temperatures where the optimisation really comes to its test. Moreover, they were built with copper coils, which are adequate for proof-of-principle studies but incompatible with steady-state operation at high magnetic field strengths. The Wendelstein 7-X (W7-X) stellarator experiment is the first representative of the new generation of optimised stellarators, and aims to show with its superconducting coil system and relatively large size (major radius 5.5 m), quasi-steady state operation with plasma parameters, including ion temperatures, close to those of a future fusion power plant [8, 9]. The sophisticated computer optimisation of W7-X came at a price, however: The coils have complicated 3D shapes, reminiscent of sculptures, Fig. 1. With today's 3D design and manufacturing techniques, complex 3-D engineering has become feasible, albeit still challenging [10]. Strict requirements for the manufacturing and assembly accuracy of the coils add to the engineering challenge, which was in fact viewed by some as unrealistic. High engineering accuracy is needed because small magnetic field errors can have a large effect on the magnetic surfaces and the confinement of the plasma.
The measurements we will present in the following confirm that the engineering challenges of building and assembling the device, in particular its coils, with the required accuracy, have been met successfully. In order to explain how this was done, we first introduce a few key concepts.

## 2 Hamiltonians, magnetic surfaces, and island chains

The equations governing magnetic field lines can be written in Hamiltonian form. It is curious that this simple, but little-known, fact was discovered only half a century ago [11], but thanks to it, the entire arsenal of Hamiltonian chaos theory can be applied to magnetic fields. For instance, the celebrated Kolmogorov-Arnold-Moser (KAM) theorem [12, 13, 14] guarantees that small perturbations to an otherwise integrable magnetic field preserve the topology of most field lines, and break it by generating so-called magnetic islands only at well-defined locations. As we shall see, these islands can be measured and visualised directly in W7-X and offer the opportunity to detect field perturbations smaller than $\delta B/B \sim 10^{-5}$. To our knowledge, it is the first time that the *topology* of a magnetic field has been measured so accurately. For more information on the theory of shaped magnetic fields and their role in plasma confinement, we refer to two recent reviews [15, 16].

A magnetic surface is not only characterised by its shape and enclosed volume, but also by its rotational transform, $\iota$. This is a measure of the poloidal rotation ("twist") of the field lines as one follows them around the magnetic surface; $\iota = 1/2$ indicates that the field line moves halfway around a magnetic surfaces in the poloidal direction for each toroidal turn it makes. Thus, for $\iota = 1/2$, the field line bites itself in the tail after two toroidal transits. Since, as shown first by Cantor, there are many more irrational than rational numbers [17], $\iota$ is typically irrational, so the magnetic field line never quite closes on itself.

## 3 Measuring the magnetic topology

Since the magnetic surface topology in a stellarator is created entirely from external coils, it can be measured in the absence of a plasma. This is done using an electron beam injected along the magnetic field. It follows and therefore maps out the magnetic field lines, and thus allows confirmation of the magnetic surface topology, flux surface mapping. As mentioned earlier, the motion along the field is much faster than the guiding-centre drifts. This is even more so for the relatively low-energy electrons used in magnetic-surface mapping. Owing to the launch of the electrons parallel to the magnetic field, and the much smaller mass of electrons relative to any ion, its ratio of parallel velocity to guiding centre drift velocity is of order 1 million. Thus, the beam follows the magnetic field lines to a very high accuracy. The source of the electron beam is an electron gun, a small negatively biassed and heated thermionic electron emitter surrounded by a small electrically grounded cylindrical structure. This electron beam alone can visualise the magnetic field line on which it is placed, through collisional excitation of a dilute background gas inside the vacuum chamber. This way, striking images can be made of the three-dimensional structure of the magnetic surfaces, see Figure 2 [18, 19].

A two-dimensional cross-sectional image generally provides clearer information though, just as Poincaré phase-space maps do for other Hamiltonian systems. Such a Poincaré plot of the magnetic surface is realised experimentally by intersecting the electron beam with a rod covered with a fluorescent, here a special zinc oxide powder (ZnO:Zn). When the rod intersects the magnetic surface on which the electron beam circulates, it fluoresces at the one or usually two locations where the rod intersects the magnetic surface and therefore collides with the electron beam. As the rod moves through the surface, all points on the latter will eventually light up. In a long camera-exposure of this sweep motion, the entire cross section of the magnetic surface appears, as shown in Figure 3. The motion of the rod itself is often invisible on such an image, since the light sources (other than the fluorescence) are kept as weak as possible. After an exposure, one can move the electron gun to another field line that defines another magnetic surface, and repeat the process. This way, the nested, closed magnetic surface topology, which is illustrated in Fig. 1, can

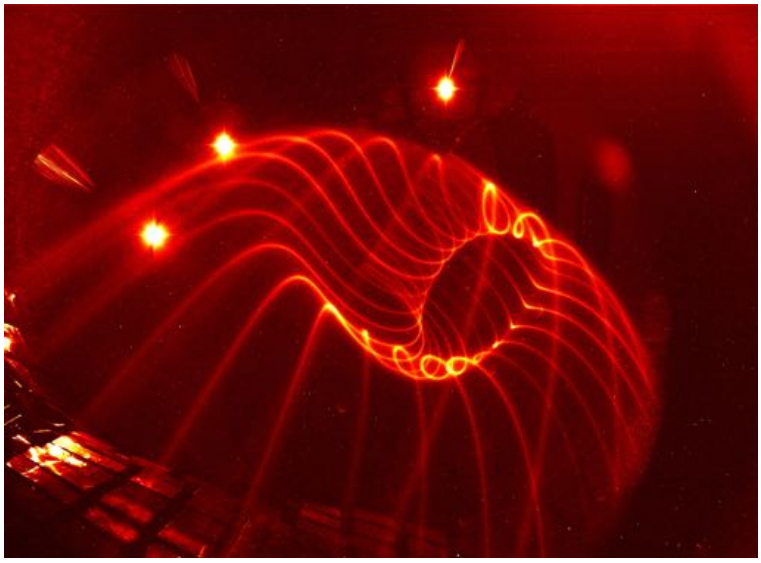

**Figure 2:** The field lines making up a magnetic surface are visualised in a dilute neutral gas, in this case primarily water vapor and nitrogen ($p_n \approx 10^{-6}$ mbar). The three bright light spots are overexposed point-like light sources used to calibrate the camera viewing geometry.

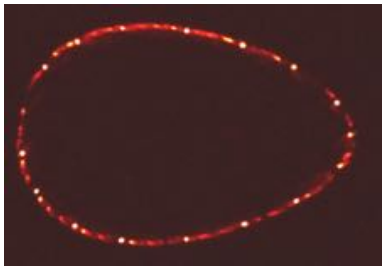

**Figure 3:** The Poincaré section of a closed magnetic surface is measured using the fluorescent rod technique. The electron beam circulates more than 40 times, ie. over 1 km along the field line.

be experimentally verified [20, 21, 22, 23], and if any magnetic island chains exist, they will show up in the Poincaré plot, as explained in the following.

## 4 Island chains and error fields

An island chain can appear on any magnetic surface with a rational value of $\iota$: a direct confirmation of the small-denominator problem in KAM theory [12]. In practice, island chains with a detectable and operation-relevant size only appear for low-order rational values of $\iota$, and only if there is a Fourier component of the magnetic field that has matching (i.e. resonant) toroidal and poloidal mode numbers, $n$ and $m$, so that $\iota = n/m$.
W7-X is designed to reach $\iota = 1$ at the outermost flux surface. It is a five-fold periodic device, with a pentagon-like shape, and thus has an $n = 5$ Fourier component to its magnetic field, so that an $n = m = 5$ island chain appears at the plasma edge. We denote unwanted field components *error fields*, and describe them in relative terms, $b_{mn} = B_{mn}/B_0$, where $B_0$ is the overall magnetic field strength, and $B_{mn}$ is the amplitude of the Fourier component of the error field. In the search for error fields, we focus on the toroidal $n$ numbers since only $n = 5$ and multiples thereof should be present, whereas a broad spectrum of poloidal $m$ numbers is present in W7-X. The $n = 1$ through

4 components are to be avoided as much as possible, in order to ensure symmetric heat load distributions onto the $2 \times 5 = 10$ divertor units to be installed at the vessel wall in future operation phases [24]. Of particular concern is the $n = 1$ component, which would create a $n/m = 1/1$ island chain.

When minimising error fields, the main engineering challenge is the geometrical precision during coil manufacturing and coil assembly. The $3.5 \times 2.5 \times 1.5$m-size non-planar coil winding packs with their five different geometries (cf. Fig. 1) are particularly critical [25]. The construction of W7-X required, for the first time, industry to manufacture superconducting coils with a highly complex shapes, with tolerances in the $\pm$1mm regime. This was accomplished by using specialised winding devices combined with precision metrology [26].

It was even more challenging to maintain the precision, and keep track of it, during installation of the coils: Positioning of the coils, machining of the contact elements, welding of mechanical supports and bolting to the massive central support ring all sums up to create an additional contribution the the error field. It was only possible to keep deviations during installation and assembly into coil groups under control by intensive use of laser-based metrology tools, systematic adjustment procedures, as well as advanced welding and machining technologies. The largest coil placement errors were less than 4.4 mm, resulting in a largest Fourier coefficient of the magnetic perturbation error of $b_{11} \approx 1.2 \cdot 10^{-4}$ [27].

## 5 Measuring error fields

Magnetic flux surface mapping, in particular of island chains [28], allows for detailed error field detection and correction [20, 29]. Island chains are sensitive indicators of small changes in the magnetic field topology, since they are physical manifestations of resonances in the magnetic topology. The radial full width $w$ of an island chain is related to a resonant magnetic field component through [16]

$$w = 4\sqrt{\frac{R_0 b_{mn}}{m(d\iota/dr)}} \Leftrightarrow b_{mn} = \frac{d\iota}{dr}\frac{w^2 m}{16 R_0}. \quad (1)$$

The width of an island chain depends on the square root of the resonant field component, $b_{mn}$, with $\iota = n/m$, and the magnetic shear $d\iota/dr$, as well as the poloidal mode number $m$ and the size of the device (via the major radius $R_0 = 5.5$ m in W7-X). In W7-X, the rotational transfrom $\iota$ is nearly constant from the inner to the outer magnetic surfaces, then $d\iota/dr$ is small, and a sizeable island chain will result from even a very small resonant error field.

With field-line mapping, island chains can be detected, and thus, $\iota$ can be determined at a specific radial location, and resonant error fields, if present, can be measured.
We show in the following that effects due to slight deformations of the magnetic coils are clearly visible, and that an important error field component in W7-X has been measured to be less than 1 in 100,000. To our knowledge, this is an unprecedented accuracy, both in terms of the as-built engineering of a fusion device, as well as in the measurement of the magnetic topology.

## 6 Adjustment of $\iota$

The magnetic topology used for initial plasma experiments in W7-X was chosen so as to avoid island chains at the plasma edge [30].

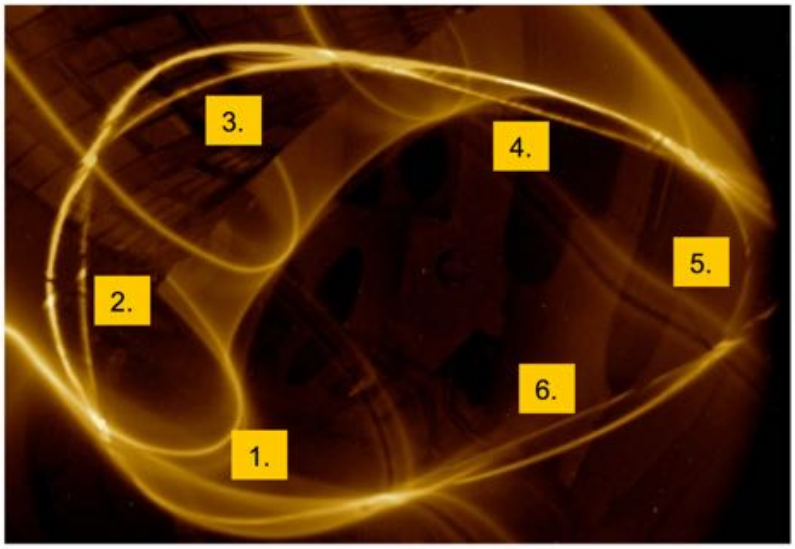


**Figure 4:** The 5/6 island chain is visible in a poloidal-radial Poincaré plot created by an electron gun and a sweep rod, as a set of six "bubbles", reflecting the $m = 6$ poloidal mode number. A thin background gas in the chamber creates a visualization of the field lines that create the x-points of the island chain.

The rotational transform $\iota$ varies from 0.79 in the centre to 0.87 at the outer magnetic surface that just touches the graphite limiters installed to protect in-vessel components by intercepting the plasma heat loads.

The $\iota = 5/6 \approx 0.83$ resonance is located inside the confinement region - and is thus unproblematic for the PFCs. It creates a prominent island chain, because of the built-in $n = 5$ component in W7-X. This island chain is indeed clearly visible, as seen in Figure 4 showing a measurement performed at the field strength $B$ =2.5 T later intended for plasma operation. The island chain location was detected almost exactly at the position expected from calculations taking the elastic deformation of the superconducting coils into account. These deformations, due to the electromagnetic forces between the magnets, cause a roughly 1% decrease in $\iota$, thus shifting the location of $\iota = 5/6$ a few cm outward from where they would be without coil deformation. This was confirmed by repeating the measurements at $B$ =0.4 T and observing that the island chain indeed appears those few centimetres further inward, Figure 5. At $B$ =0.4 T, the electromagnetic forces are $(2.5/0.4)^2 \approx 39$ times smaller than at $B$ =2.5 T. The actual change in the angle of the magnetic field vector detected in this way is only about 0.1%. Nevertheless, it shows up in Fig. 5 as a clearly visible radial shift of the island chain. A more detailed analysis of these data can be found elsewhere [31].

## 7 Evaluation of an n=1, m=2 error field

For the first measurements of the $n = 1$ error field, a special magnetic surface configuration was used [32], where $\iota$ varies slowly and passes through the resonance $\iota = 1/2$, see Fig. 6.

In the complete absence of error fields, a small $n = 5$, $m = 10$ island chain would appear at the $\iota = 1/2$ location at around 25 cm distance from the innermost magnetic surface, but in the presence of even a small $n = 1$ error field, an $n = 1$, $m = 2$ island chain, visible in a Poincaré plot as two "bubbles" will appear.

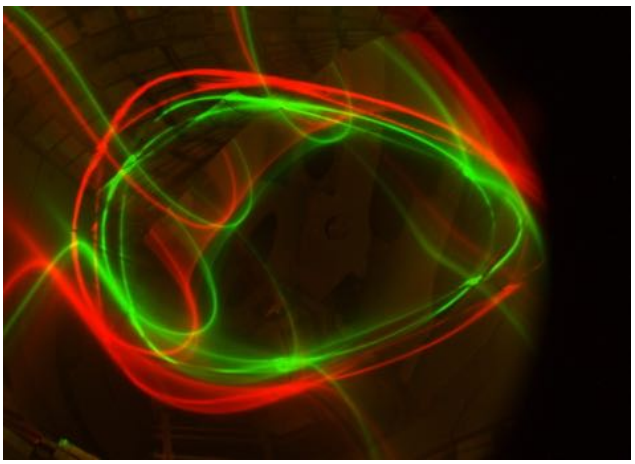

**Figure 5:** The 5/6 island chain is shown in green for $B$ =0.4 T, and in red for $B$ =2.5 T. Although nominally one might expect them to be identical, the 5/6 island chain is further out at high field strength, due to small deformations of the magnet coils under electromagnetic forces.

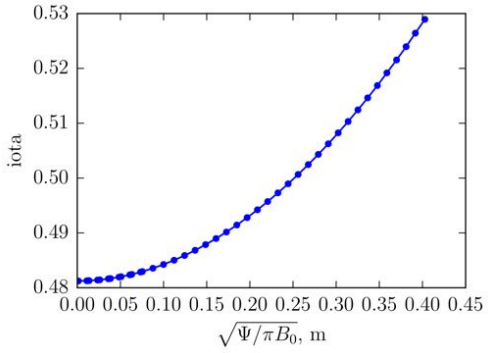


**Figure 6:** The $\iota$ profile is shown for the special configuration developed for field error detection. $\iota$ varies only minimally around the resonant value of 1/2.

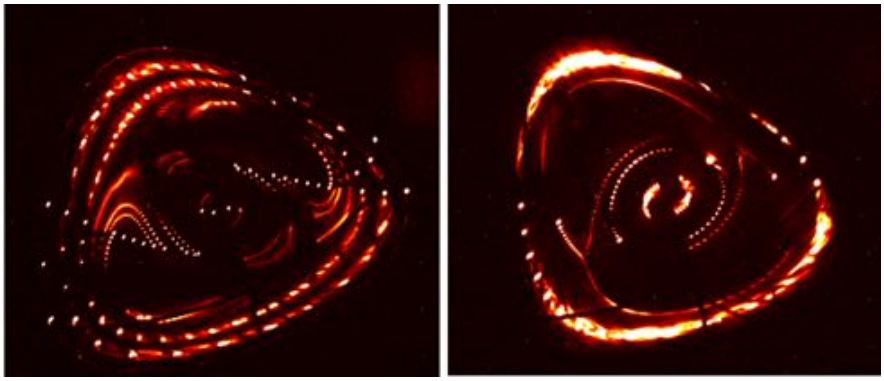

**Figure 7:** For the special $\iota \approx 1/2$ configuration, the $m = 2$, $n = 1$ island size and phase can be measured by the Poincaré section method. Here two conglomerate images with several nested surfaces are shown for two different phases of a purposely added $n = 1$ field structure with the same amplitude. Although the shadowing problem leads to gaps, the trained eye can still detect the changes in size and phase of the $m = 2$ island.

The $b_{21}$ error field is too small to create an island structure large enough to be measured clearly. This is in part due to the good news that it is small, and in part due to $\iota$ being so close to 1/2, that the electron beam comes very close to its launch position (the electron gun) after two toroidal transits, thus running the risk of hitting the back of the electron gun and disappearing.

It is nevertheless possible to indirectly measure the $b_{21}$ field error, despite this shadowing problem, by adding an $n = 1$ error field with a well-defined amplitude and phase, using the set of large external coils [33] shown in yellow in Figure 1. The primary purpose of these coils is to trim away the unwanted $n = 1$ error field components, but the trim coils are used here to *create* an extra $n = 1$ error field, and thus generate an $n/m = 1/2$ island chain wide enough to be measurable.

By scanning the phase and amplitude of the imposed, well-defined error field, measuring the island phase and width (Fig. 7), and comparing to Equation 1, we find that a $n/m = 1/2$ island with a width of 4 cm must be present, even in the absence of trim-coil induced fields. The configuration has $d\iota/dr \approx 0.15\ \mathrm{m}^{-1}$ at the $\iota = 1/2$ location, so using Equation 1 again, we arrive at $b_{21} \approx 5.4{\cdot}10^{-6}$. This value is well within the range that can be corrected with the trim coils [33] and is even on the low side of what was estimated from metrology. Measurement and correction of the closely related, and for future operation much more critical, error field component $b_{11}$, are planned for the near future, using an $\iota \approx 1$ configuration [34]. Since the $b_{11}$ and the $b_{21}$ components should be of the same order of magnitude, the 1/1 error fields are also expected to be small - certainly within the correction capabilities of the W7-X coil set.

## 8 Summary

The need for complex 3D shaping and high-accuracy requirements have been viewed as major problems for optimised stellarators. Wendelstein 7-X demonstrates that a large, optimised, superconducting stellarator can be built with the required accuracy to generate good magnetic surfaces with the required topology, and that experimental tools exist to verify this fact and to further fine-tune the magnetic topology. These results were obtained using magnetic field-line mapping, a sensitive technique to measure the detailed topology of the magnetic surfaces. To reach the other goals of the device, and provide an answer to the question "is the stellarator the right concept for fusion energy?", years of plasma physics research is needed. That task has just started.

# 9 Acknowledgements

This work has been carried out within the framework of the EUROfusion Consortium and has received funding from the Euratom research and training programme 2014-2018 under grant agreement No 633053. The views and opinions expressed herein do not necessarily reflect those of the European Commission. SL acknowledges support from US DOE grant DE-AC02-09CH11466. TSP would like to thank U. Nielsen and K. Søndergaard Larsen for useful suggestions to improve the text.

# References

[1] Lawson, J. D. Some Criteria for a Power Producing Thermonuclear Reactor. *Proc. Phys. Soc. B* **70**, 6-10 (1957).

[2] Lorenzini, R. *et al.* Self-organized helical equilibria as a new paradigm for ohmically heated fusion plasmas. *Nature Physics* **5**, 570-574 (2009).

[3] Spitzer, L. The stellarator concept. *Phys. Fluids* **1**, 253-264 (1958).

[4] Nührenberg, J., Zille, R. Quasi-helically symmetric toroidal stellarators. *Phys. Lett. A* **129**, 113-117 (1988).

[5] Boozer, A. H. Plasma equilibrium with rational magnetic surfaces. *Phys. Fluids* **24**, 1999-2003 (1981).

[6] Canik, F. M. *et al.* Experimental Demonstration of Improved Neoclassical Transport with Quasi-helical Symmetry. *Phys. Rev. Lett.* **98**, 085002 (2007).

[7] Hirsch, M. *et al.* Major results from the stellarator Wendelstein 7-AS. *Plasma Phys. Contr. Fusion* **50**, 053001 (2008).

[8] Beidler, C. *et al.* Physics and Engineering Design for Wendelstein VII-X. *Fusion Sci. Technol.* **17**, 148-168 (1990).

[9] Nührenberg, J., Zille, R. Stable stellarators with medium $\beta$ and aspect ratio. *Phys. Lett. A* **114**, 129-132 (1986).

[10] Bosch, H. S. *et al.* Technical challenges in the construction of the steady-state stellarator Wendelstein 7-X. *Nucl. Fusion* **53**, 126001 (2013).

[11] Kerst, D. W. The influence of errors on the plasma confining magnetic field. *J. Nucl. Energy C* **4**, 253-262 (1962).

[12] Kolmogorov, A. N. On conservation of conditionally periodic motions for a small change in Hamilton's function. *Dokl. Akad. Nauk. SSSR* **98**, 527-530 (1954).

[13] Arnold, V. I. Small denominators and problems of stability of motion in classical and celestial mechanics. *Russ. Math. Surv.* **18**, 85-191 (1963).

[14] Moser, J. On Invariant Curves of Area-Preserving Mappings of an Annulus. *Nachr. Akad. Wiss. Göttingen* **II**, 1-20 (1962).

[15] Helander, P. Theory of plasma confinement in non-axisymmetric magnetic fields. *Rep. Prog. Phys.* **77**, 087001 (2014).

[16] Boozer, A. H. Non-axisymmetric magnetic fields and toroidal plasma confinement. *Nucl. Fusion* **55**, 025001 (2015).

[17] Cantor, G. Ueber eine Eigenschaft des Inbegriffes aller reellen algebraischen Zahlen. *J. Reine Angew. Math.* **77**, 258-262 (1874).

[18] Brenner, P. W., Pedersen, T. S., Berkery, J. W., Marksteiner, Q. R., Hahn, M. S. Magnetic Surface Visualizations in the Columbia Non-Neutral Torus. *IEEE Trans. Plasma Sci.* **36**, 1108-1109 (2008).

[19] Drewelow, P., Bräuer, T., Otte, M., Wagner, F. Three-dimensional photogrammetric measurement of magnetic field lines in the WEGA stellarator. *Rev. Sci. Instrum.* **80**, 123501 (2009).

[20] Sinclair, R. M., Hosea, J. C., Sheffield, G. V. Magnetic surface mappings by storage of phase-stabilized low-energy electron beams. *Appl. Phys. Lett.* **17**, 92-95 (1970).

[21] Dikij, A. G. *et al.* ORNL Report No. TR-86/29, (1986).

[22] Hartwell, G. J. *et al.* Magnetic surface mapping with highly transparent screens on the Auburn torsatron *Rev. Sci. Instrum.* **59**, 460-466 (1988).

[23] Jaenicke, R., Ascasibar, E., Grigull, P., Lakicevic, I., Weller, A., Zippe M. Detailed investigation of the vacuum magnetic surfaces on the W7-AS stellarator. *Nucl. Fusion* **33**, 687-704 (1993).

[24] Renner, H. *et al.* Physical Aspects and Design of the Wendelstein 7-X Divertor. *Fusion Sci. Technol.* **46**, 318-326 (2004).

[25] Rummel, T., *et al.* The Superconducting Magnet System of the Stellarator Wendelstein 7-X. *IEEE Trans. Plasma Sci.* **40**, 769-776 (2012).

[26] Andreeva, T., Bräuer, T., Endler, M., Kißlinger, J., v. Toussaint, U. Influence of construction errors on Wendelstein 7-X magnetic configurations. *Fusion Eng. Des.* **88**, 408-412 (2009).

[27] Andreeva, T., *et al.* Tracking of the magnet system geometry during Wendelstein 7-X construction to achieve the designed magnetic field. *Nucl. Fusion* **55**, 063025 (2015).

[28] Berezhetskii, M. S., Grebenshchikov, S. E., Popryadukhin, A. P., Shpigel, I. S. Magnetic Surfaces and Containment of a Plasma by Spiral Fields in a Stellarator with External Injection. (in Russian), *J. Tech. Phys.* **35**, 2167 (1965). English translation: *Sov. Phys. Tech. Phys.* **10**, 1662 (1966).

[29] Colchin, R. J., *et al.* Electron beam and magnetic field mapping techniques used to determine field errors in the ATF torsatron. *Rev. Sci. Instrum.* **60**, 2680-2689 (1989).

[30] Pedersen, T. S. *et al.* Plans for the first plasma operation of Wendelstein 7-X. *Nucl. Fusion* **55**, 126001 (2015).

[31] Otte, M. *et al.* Setup and Initial Results from the Magnetic Flux Surface Diagnostics at Wendelstein 7-X. Submitted to *Plasma Phys. Contr. Fusion* (2016).

[32] Lazerson, S. *et al.* First measurements of error fields on W7-X using flux surface mapping. Submitted to *Nucl. Fusion* (2016).

[33] Rummel, T. *et al.* The Trim Coils for the Wendelstein 7-X Magnet System. *IEEE Trans. Appl. Supercond.* **22**, 4201704 (2012).

[34] Bozhenkov, S. A. *et al.* Methods for measuring 1/1 error field in Wendelstein 7-X stellarator. Submitted to *Nucl. Fusion* (2016).